EARTH SURFACE PROCESSES AND LANDFORMS
Earth Surf. Process. Landforms **43**, 1169–1182 (2018)

Published online 5 December 2017 in Wiley Online Library
(wileyonlinelibrary.com) DOI: 10.1002/esp.4267

Morphodynamic assessment of side channel systems using a simple one-dimensional bifurcation model and a comparison with aerial images

R. Pepijn van Denderen,[1]* Ralph M. J. Schielen,[1,2] Astrid Blom,[3] Suzanne J. M. H. Hulscher[1] and Maarten G. Kleinhans[4]
[1] Faculty of Engineering Technology, University of Twente, Enschede, The Netherlands
[2] Ministry of Infrastructure and Water Management Rijkswaterstaat, Utrecht, The Netherlands
[3] Faculty of Civil Engineering and Geosciences, Delft University of Technology, Delft, The Netherlands
[4] Faculty of Geosciences, Utrecht University, Utrecht, The Netherlands

Received 19 December 2016; Revised 14 September 2017; Accepted 21 September 2017

*Correspondence to: R. Pepijn van Denderen, Faculty of Engineering Technology, University of Twente, Enschede, The Netherlands. E-mail: r.p.vandenderen@utwente.nl

ESPL
Earth Surface Processes and Landforms

ABSTRACT: Side channel construction is a common intervention applied to increase a river's conveyance capacity and to increase its ecological value. Past modelling efforts suggest two mechanisms affecting the morphodynamic change of a side channel: (1) a difference in channel slope between the side channel and the main channel and (2) bend flow just upstream of the bifurcation. The objective of this paper was to assess the conditions under which side channels generally aggrade or degrade and to assess the characteristic timescales of the associated morphological change. We use a one-dimensional bifurcation model to predict the development of side channel systems and the characteristic timescale for a wide range of conditions. We then compare these results to multitemporal aerial images of four side channel systems. We consider the following mechanisms at the bifurcation to be important for side channel development: sediment diversion due to the bifurcation angle, sediment diversion due to the transverse bed slope, partitioning of suspended load, mixed sediment processes such as sorting at the bifurcation, bank erosion, deposition due to vegetation, and floodplain sedimentation. There are limitations to using a one-dimensional numerical model as it can only account for these mechanisms in a parametrized manner, but the model reproduces general behaviour of the natural side channels until floodplain-forming processes become important. The main result is a set of stability diagrams with key model parameters that can be used to assess the development of a side channel system and the associated timescale, which will aid in the future design and maintenance of side channel systems. © 2017 The Authors. Earth Surface Processes and Landforms published by John Wiley & Sons Ltd.

KEYWORDS: side channel; bifurcation; morphodynamic modelling; stability; river morphodynamics

Introduction

A *side channel system* is a term for a two-channel system that is connected at both ends, in which the side channel conveys much less discharge than the main channel. In the past, many side channel systems disappeared due to human interference, which resulted in a loss of habitat diversity and a decrease in the conveyance capacity of the river. In several rivers in Europe and North America, restoration projects aim to restore the river to a more natural state, and such stream restoration may include the construction of side channels. The main objectives of side channel construction are to improve flood safety (Simons *et al.*, 2001; Nabet, 2014), to increase ecological value (Schiemer *et al.*, 1999; Formann *et al.*, 2007), to restore river branches (Henry *et al.*, 1995; Helfield *et al.*, 2012) and to reduce degradation in the main channel (Tockner *et al.*, 1998; Formann *et al.*, 2007). However, side channels often suffer from aggradation or degradation, which results in the need for regular maintenance. This is both expensive and can deteriorate the targeted ecosystem, and therefore a side channel without the need for intensive maintenance is desirable. However, it is unclear whether such a maintenance-free side channel system can exist. A better understanding of the mechanisms that influence morphodynamic changes of side channel systems is therefore needed.

Side channels also occur in natural rivers in the form of, for example, cutoff channels and chute channels. After the initiation of such a new channel, various mechanisms determine the discharge and sediment partitioning at the bifurcation, which in turn determine the development of

the two-channel system (Slingerland and Smith, 1998, 2004; Van Dijk *et al.*, 2012). A cutoff channel that becomes the dominant channel reduces the transport capacity in the main channel, leading to aggradation in the main channel (Constantine *et al.*, 2010; Van Dijk *et al.*, 2012). This aggradation can be distributed over the channel (Dieras *et al.*, 2013) or if, for example, the bifurcation angle is large, local deposition at the entrance of the channel may lead to the formation of a plugbar. After the main channel is closed due to a plugbar, it slowly silts up through deposition of fine sediment due to overbank flow (Constantine *et al.*, 2010; Toonen *et al.*, 2012). From the moment that the discharge in the closing channel is limited, a return current in the side channel can form due to water-level variations at the confluence. This can increase the aggradation rate of the closing channel (Citterio and Piégay, 2009; Le Coz *et al.*, 2010).

The stability of a bifurcation is determined by the sediment supply to the downstream branches and their sediment transport capacity (Wang *et al.*, 1995). There are several mechanisms that affect the sediment supply and the transport capacity of the downstream branches: a difference in slope between the side channel and the main channel (Bolla Pittaluga *et al.*, 2003), sediment diversion due to bend flow (Kleinhans *et al.*, 2008; Van Dijk *et al.*, 2014), sediment diversion due to a transverse bed slope at the bifurcation (Bolla Pittaluga *et al.*, 2003; Kleinhans *et al.*, 2008), sediment diversion due to the bifurcation angle (Bulle, 1926; Van der Mark and Mosselman, 2013; Dutta *et al.*, 2017), partitioning of suspended load (Slingerland and Smith, 1998, 2004; Edmonds and Slingerland, 2008; Gaweesh and Meselhe, 2016), mixed sediment processes (Sloff *et al.*, 2003; Frings and Kleinhans, 2008; Sloff and Mosselman, 2012; Kästner *et al.*, 2017), bank erosion (Miori *et al.*, 2006; Kleinhans *et al.*, 2011), deposition due to vegetation (Rodrigues *et al.*, 2006) and floodplain sedimentation (Toonen *et al.*, 2012). The discharge partitioning at the bifurcation is proportional to the water surface slope in the downstream channels and is therefore related to the length of the channels (Mendoza *et al.*, 2016). The sediment partitioning at the bifurcation is related to the discharge partitioning and is among other things affected by a transverse bed slope (Bolla Pittaluga *et al.*, 2003) and bend flow (Kleinhans *et al.*, 2008). Bend flow creates a secondary flow that at the water surface is directed toward the outer bend and at the bed towards the inner bend (Dietrich and Smith, 1984; Struiksma *et al.*, 1985). If a bifurcation is located just downstream of a bend (Figure 1), the sediment transport is slightly directed towards the channel in the inner bend (Kleinhans *et al.*, 2008; Hardy *et al.*, 2011; Van Dijk *et al.*, 2014). The transverse bed slope results from a difference in bed level between the downstream branches that influences the bed level up to a certain distance upstream of the bifurcation. This transverse slope deflects sediment into the deeper channel due to the gravity effect (Bolla Pittaluga *et al.*, 2003; Kleinhans *et al.*, 2008). Both bend flow and the transverse bed slope affect the partitioning of bed load at the bifurcation. Suspended bed-material load is less affected by slope effects and the sediment concentration varies less with vertical distance from the bed than bed load (Church, 2006), which means that vertical differences in flow direction also have a smaller influence on the partitioning of suspended bed-material load. Wash load is almost uniformly distributed over the depth (Bridge, 2003). The partitioning of wash load is therefore expected to be about the same as the discharge partitioning.

The bifurcation angle is the angle between the side channel and main channel (Figure 1) and is defined at the intersection between the centrelines of the downstream channels. The

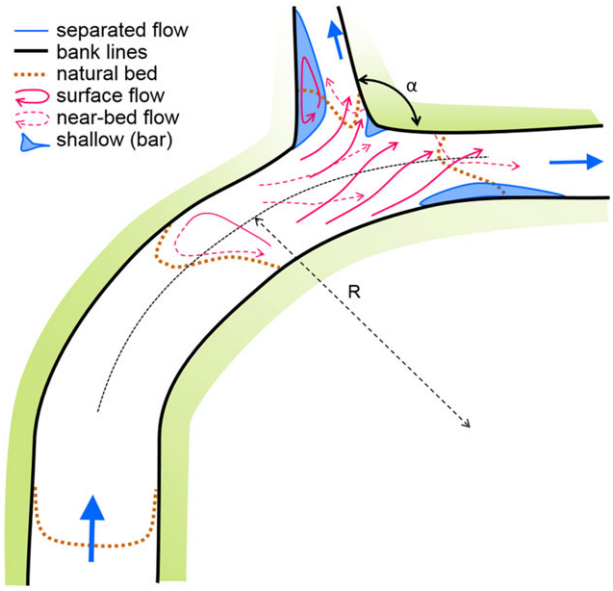

Figure 1. Flow patterns at a bifurcation that is located downstream of a river bend with radius R and bifurcation angle (α) is such that flow separation occurs. (After Kleinhans *et al.*, 2013.). [Colour figure can be viewed at wileyonlinelibrary.com]

diversion of the flow towards the side channel is associated with a spiral flow upstream of the bifurcation in which the velocity near the bed is directed towards the side channel. This increases the sediment load towards the side channel, which is also known as the Bulle effect (Bulle, 1926; Riad, 1961; Van der Mark and Mosselman, 2013). It is expected that the Bulle effect increases with an increasing bifurcation angle (De Heer and Mosselman, 2004; Van der Mark and Mosselman, 2013; Dutta *et al.*, 2017). However, for large bifurcation angles a flow separation zone may develop (Figure 1) (Bulle, 1926; Riad, 1961; Constantine *et al.*, 2010; Dutta *et al.*, 2017). If flow separation occurs, the influence of the Bulle effect on the sediment partitioning seems small compared to the influence of the flow separation zone (De Heer and Mosselman, 2004; Van der Mark and Mosselman, 2013). Due to the smaller flow velocities and the circulation inside the flow separation zone, a bar forms inside this zone (Constantine *et al.*, 2010; Zinger *et al.*, 2013). The reduced effective width increases the flow velocities at the entrance of the side channel (Figure 1), causing large scour and, potentially, bank erosion (Kleinhans *et al.*, 2013; Zinger *et al.*, 2013). However, if the side channel attracts only a limited amount of discharge, large deposition in the separation zone may lead to a plugbar (Constantine *et al.*, 2010; Kleinhans *et al.*, 2013).

Bank erosion and accretion influence the timescale of bifurcation development (Kleinhans *et al.*, 2011). Width adaptation allows for a larger difference in discharge between the downstream branches than without width adaptation (Miori *et al.*, 2006). In a degrading channel, bank erosion adds more sediment to the channel, thus reducing the amount of sediment that is picked up from the bed (Kleinhans *et al.*, 2011). On the other hand, in the case of bank accretion sediment is deposited on the sides of the channel reducing the amount of sediment deposited in the middle of the channel. This means that the time after which an equilibrium flow depth is reached increases.

The dynamics of bifurcations have been studied using various models. One-dimensional modelling of bifurcation behaviour requires a relation for the sediment partitioning that accounts for two-dimensional (2D) and three-dimensional (3D) effects on the sediment partitioning in a parametrized way. The sediment partitioning is expected to be related to the

characteristics of the downstream channels (Riad, 1961; Wang *et al.*, 1995). After introducing a more extended nodal point relation, Wang *et al.* (1995) introduce a strongly simplified relation and use this in a linear stability analysis:

$$\frac{Q_{s2}}{Q_{s3}} = \left(\frac{Q_2}{Q_3}\right)^k \left(\frac{W_2}{W_3}\right)^{1-k} \tag{1}$$

where Q_{si} is the sediment load delivered to the downstream branch i (where $i \in [2, 3]$ indicates each of the downstream branches), Q_i is the water discharge in branch i, W_i is the width in branch i and k is an empirical parameter. It was found that for $k > n/3$ the bifurcation is stable and for $k < n/3$ the bifurcation is unstable (Wang *et al.*, 1995), which implies that one of the downstream branches closes. The parameter n is the degree of nonlinearity of the sediment transport relation ($Q_s \propto u^n$) and $n = 5$ for Engelund and Hansen (1967). A case with $k < n/3$ implies that a small increase of the discharge in branch i leads to a small increase of the sediment supply to branch i and at the same time a relatively large increase of the transport capacity, which results in degradation. This increases the discharge even more, which implies that the bifurcation is unstable. A case with $k > n/3$ implies that a small increase of the discharge in branch i leads to an increase of the sediment supply that is larger than the increase of the sediment transport capacity, which results in aggradation. The aggradation decreases the discharge to this branch and leads to a stable bifurcation. A model for k is still lacking, which complicates the application of Equation (1) to natural cases.

A second model to study bifurcation dynamics is proposed by Bolla Pittaluga *et al.* (2003). The model is based on a mass balance over two computational cells upstream of the bifurcation between which a transverse sediment flux occurs. This flux occurs due to: (a) the fact that the discharge partitioning generally differs from the width ratio (Q_y in Equation (A7)); (b) the transverse bed slope associated with a difference in bed level between the downstream branches (Bolla Pittaluga *et al.*, 2003); (c) the presence of bend flow upstream of the bifurcation (Kleinhans *et al.*, 2008). A degrading deeper channel leads to a larger transverse bed slope and therefore a larger sediment supply. This continues until an equilibrium is reached and results in an asymmetric stable bifurcation in which neither branch is forced to close. The transverse bed slope therefore has a stabilizing effect. The magnitude of the transverse bed slope effect is a function of the Shields parameter, the width-to-depth ratio and the bed-level difference between the downstream channels (Bolla Pittaluga *et al.*, 2003, 2015). Several laboratory experiments and field cases show that such stable asymmetric bifurcations can occur in cases that are dominated by bed load (Bertoldi and Tubino, 2007; Kleinhans *et al.*, 2008; Bolla Pittaluga *et al.*, 2015). If the transverse bed slope and the bend flow are ignored, the nodal point relation of Bolla Pittaluga *et al.* (2003) reduces to Equation (1) with $k = 1$.

The objective of this paper is to assess the conditions under which side channels generally aggrade or degrade and to assess the characteristic timescales of the associated morphological change. We use a one-dimensional bifurcation model to predict the development of side channel systems and the associated timescale for a range of conditions, and generalize these in the form of stability diagrams with the most important model parameters. We then compare these results with aerial images that show the development of four side channel systems to test whether the model reproduces these configurations. First we introduce the model and explain how we use it. In the Results section we first show the predicted side channel development and then we compare these results to the observed development of the four side channel systems.

Model Description

We use the one-dimensional numerical bifurcation model developed by Kleinhans *et al.* (2011). The model consists of four branches: the upstream channel, the main channel, the side channel parallel to the main channel and the recombined downstream channel. The length of each branch is assumed to be constant in the model. A constant bankfull discharge is imposed at the upstream boundary, and at the downstream end a constant water level is imposed. Floodplain processes and effects on flow division are excluded and Kleinhans *et al.* (2008) showed that discharge fluctuations then have a negligible effect on the development of such well-defined bifurcating channels. The discharge partitioning at the bifurcation is computed by numerically solving the flow depth at the bifurcation using the backwater equation (Parker, 2004) under the condition that the water levels at the upstream end as well as the downstream end, where they recombine, of the side channel and main channel are equal. The sediment transport is computed using the sediment transport relation by Engelund and Hansen (1967). The sediment partitions at the bifurcation based on the nodal point relation by Bolla Pittaluga *et al.* (2003) (see Appendix) with an adjustment of the transverse sediment transport due to a river bend upstream of the bifurcation (Kleinhans *et al.*, 2011). To account for width adaptation of the channels, an empirical equilibrium width is computed based on the discharge in the channel (Equation (A8)). The sediment that is added or removed from the banks is accounted for as a source or sink term in the Exner conservation law (Equation (A11)).

As a constant bankfull discharge overestimates the yearly averaged sediment transport rate of the river, the model underestimates the timescale of the side channel development. We introduce an intermittency factor that corrects for the nonlinear behaviour of the sediment supply in relation to the water discharge (Parker, 2004; Kleinhans *et al.*, 2011). We define the intermittency factor as the measured yearly-averaged sediment transport rate of the river divided by the yearly-averaged sediment transport rate as estimated with bankfull discharge.

Two additional mechanisms are accounted for in this paper. Firstly, we assume a fraction μ of the sediment supply that is unaffected by bed slope effects or bend flow. This fraction is therefore related to the limited effect of a transverse bed slope or bend flow at the bifurcation on suspended load. Secondly, we account for the effects of flow separation with a simple parametrization of the reduction of the effective entrance width caused by the separated flow cell. The size of the flow separation zone is estimated by (Constantine *et al.*, 2010)

$$\epsilon = 1 - 0.94e^{-0.013\alpha} \tag{2}$$

where ϵ is a fraction of the channel width that is occupied by the flow separation zone and α is the diversion angle in degrees. This relation is based on model results in which the shape of the bifurcation is abrupt (Constantine *et al.*, 2010). The sediment load that enters the flow separation zone (Q_{sf}) is estimated by

$$Q_{sf} = \epsilon Q_{si} \tag{3}$$

where Q_{si} is the total amount of sediment supplied to branch i. The length of the flow separation zone is unknown, but as a first estimate we assume that the length of the flow separation zone is the same size as the first grid cell (Δx). This leads to

$$\frac{\partial W_{x0}}{\partial t} = \frac{1}{h}\frac{Q_{sf}}{\Delta x} \tag{4}$$

where W_{x0} is the width of the channel entrance and h is the flow depth at the entrance of the channel. From this it follows that the size and growth rate of the bar at the entrance of the

Table I. List of side channel systems with their main characteristics

River	Location	L_{side}/L_{main} (m m^{-1})	Q_{bank} (m^3 s^{-1})	W_{bank} (m)	D_{50} (mm)	k (m)	Fr	θ	$Q_{s,yearly}$ (m^3 yr^{-1})	Reference
Ain, France	Mollon (45° 56′ 51.14″ N; 5° 14′ 55.36″ E)	1600/1800	400	80	30	0.33[a]	0.38	0.06	60 000	Bravard (1986); Rollet (2007); Olivier *et al.* (2009); Dieras *et al.* (2013)
	Martinaz (45° 56′ 5.14″ N; 5° 15′ 9.72″ E)	950/1000	400	80	30	0.33[a]	0.38	0.06	60 000	
Sacramento River, USA	Colusa (39° 19′ 31.35″ N; 122° 1′ 31.28″ W)	1200/1900	1840	259	2	0.7[b]	0.2	0.48	1 500 000	Singer and Dunne (2004); Constantine *et al.* (2010)
Wabash River, USA	Mackey Bend (37° 48′ 57.99″ N; 88° 2′ 29.52″ W)	2500/11 500	2000	300	0.7	0.12[c]	0.2	0.40	1 320 000	Zinger *et al.* (2011, 2013); Konsoer (2014); Zinger (2016)

Note: L_{side}/L_{main} is the length of the two channels in which the side channel is the initially smallest channel, Q_{bank} and W_{bank} are the bankfull discharge and width, D_{50} is the median grain size, k is the Nikuradse roughness length and $Q_{s,yearly}$ is the average annual sediment load of the river.

[a]Based on water depth and discharge measurements.

[b]Based on bankfull discharge, width and velocity estimation (Constantine *et al.*, 2010).

[c]Nikuradse roughness length was estimated using the ripple roughness height relation (Van Rijn, 1993), based on the measured dune height and length in the upstream channel (Zinger, 2016) during a discharge of 1565 m^3 s^{-1}.

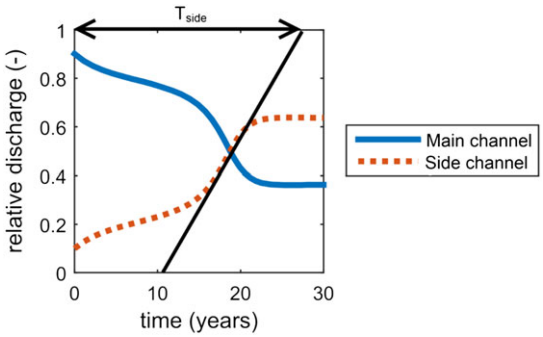

Figure 2. An example of the calculation method of the timescale of side channel development. A tangent line is drawn at the location where the gradient in the discharge is largest. This timescale is then made dimensionless by Equation (5). [Colour figure can be viewed at wileyonlinelibrary.com]

bifurcation is a function of the grid cell size Δx. We recognize that this approach is not appropriate as the discretization may not affect the results. It is a pragmatic choice that will need to be reformulated and improved in future analyses.

Method

We compute the side channel development and the corresponding timescale for a range of side channel characteristics, including three rivers: the river Ain, the Wabash River and the Sacramento River (Table I). We then compare these results with observed development of the side channel systems in these rivers.

Assessment of general side channel behaviour

We use the one-dimensional numerical model described above to study the general development of side channel systems. We compute the development for the three selected rivers (Table I) and we vary five model parameters between reasonable ranges to study the stability of the side channel system. These model parameters are the length of the side channel, bend flow at the bifurcation, bank erosion, the bifurcation angle, and the fraction of suspended bed-material load. We assume the initial water discharge into the side channel to be 10% and into the main channel equal to 90%. The effect of this assumption on the result appears to be limited for small variations of the initial condition. Based on this initial discharge and assuming an equilibrium water depth in each branch, we estimate the initial bed level. We assume that an equilibrium is reached when the discharge changes less than 0.5 m^3 s^{-1} between subsequent years. The timescale of the side channel development is estimated based on the tangent line at the largest gradient in the time–discharge results of the side channel (Figure 2). The timescale is non-dimensionalized using the yearly averaged sediment supply and the initial volume of the side channel ($V_{side} = W_{side}L_{side}h_{side}$):

$$T_{ref} = \frac{T_{side}}{\frac{W_{side}}{W_{main}+W_{side}} Q_{s,yearly} W_{side} L_{side} h_{side}} \tag{5}$$

where $Q_{s,yearly}$ is the yearly averaged sediment supply, W_{side} is the initial width of the side channel, L_{side} is the length of the side channel from the bifurcation to the confluence and h_{side} is the initial flow depth of the side channel.

Use of aerial images

We study four side channel systems using aerial image time series (Table I). We selected these four sites because their side channel development is visible from the time series and human influence on their development seems limited. The length of a channel is measured following its centreline. Using the aerial images, we study the locations of deposition and scour, the timescale of side channel development and channel migration. We then pose several hypotheses for mechanisms that determine or affect the morphodynamic change in the side channel systems. The results of the one-dimensional (1D) model are used to quantify the effects of the mechanisms on the stability of the side channel system and the timescale of the side channel development.

Results

General side channel development

We apply 1D numerical model described in above to estimate the equilibrium state of a side channel system. According to the model, the length of the side channel relative to that of the main channel strongly determines the side channel development (Figure 3). If the side channel is much shorter than the main channel, the side channel becomes the dominant channel. Neither channel fully closes, because at some point the transverse bed slope is large enough to divert a sufficient amount of sediment from the shallower channel to the deeper channel such that the transport capacity in each downstream channels is equal to its sediment supply. There is an abrupt transition between the dominance of the side channel and the dominance of the main channel. This abrupt transition is caused by the transverse bed slope effect. A situation with an equal discharge in both branches is unstable due to a small transverse bed slope. These results show that the transition between a dominant side channel and a dominant main channel occurs for similar length ratios for a sand-bed river such as the Wabash River, a sand-gravel river such as the Sacramento River and a gravel-bed river such as the river Ain. With increasing discharge asymmetry, the transverse bed slope increases until the sediment supply to the channel matches its sediment transport capacity. The stability of the bifurcation and the location of the transition therefore depend on the magnitude ($\partial\eta/\partial y$) and the intensity ($1/f(\theta)$) of the transverse bed slope effect (Equation (A3)), which agrees with previous studies (Bolla Pittaluga *et al.*, 2003, 2015). This causes the transition to occur at slightly different values for the three rivers. The transition for the Sacramento River occurs at a slightly lower length ratio, because the high Shields parameter reduces the transverse bed slope effect (Table I).

We extend this analysis with the effect of bend flow at the bifurcation (Figure 4A–D). If the side channel is located in an inner bend, more sediment is supplied to the side channel compared to a case with a straight upstream channel, and therefore it is likely that the main channel becomes dominant (Figure 4A). Similarly, when the side channel is located in the outer bend, it receives less sediment and it is more likely that the side channel becomes dominant (Figure 4B). The abrupt transition (Figure 3) is shown as a white line in these graphs. The smaller transverse bed slope effect in the Sacramento River shifts the transition to lower values of the length ratio. The transition for the river Ain is similar to the Wabash River for gradual bends, but with a decreasing relative radius the intensity of the bend flow increases faster for the river Ain due to a larger depth–width ratio (Equation (A6)).

The results change slightly if the width adaptation of the downstream branches is accounted for (Figure 4C, D). The width adaptation is assumed to be a function of the flow rate (Equation (A8)) and a degrading channel will therefore increase in width. This increases the timescale of the side channel development since the eroded sediment acts as source of sediment in the Exner conservation law. The flow depth in a degrading channel increases less with an increase of discharge compared to the case without width adaptation. This also leads to a smaller difference in bed level between the downstream channels and therefore a smaller transverse bed slope. The side channel system therefore stabilizes at a larger discharge asymmetry and it is easier to switch from a dominant main channel to a dominant side channel, which results in a shift of the transition zone. This is shown in Figure 4D as an upward shift of the transition line at large length ratios. In the case of a side channel in the inner bend and width adaptation (Figure 4C), a large transition zone occurs, because due to bend flow the upstream channel supplies sufficient sediment to the side channel to match its increased transport capacity. This does not occur in the case without width adaptation, because the transverse sediment transport due to bend flow increases with a decreasing width difference between the downstream branches (Equation (A5)).

The timescale of side channel development (Equation (5)) depends on the transport capacity in and the sediment supply to each branch (Figure 5). The maximum timescale goes theoretically to infinity because there are conditions under which the supplied sediment matches the transport capacity of the channels. However, the model results are discrete and

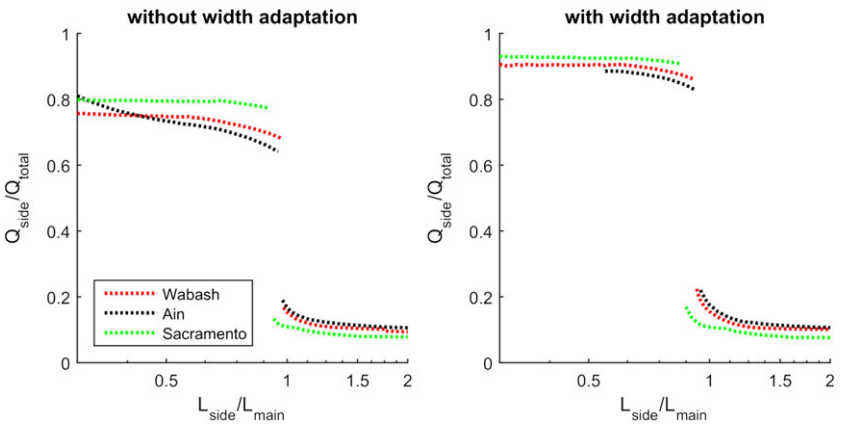

Figure 3. Equilibrium discharge partitioning for three rivers as a function of the length difference between the side channel and the main channel. [Colour figure can be viewed at wileyonlinelibrary.com]

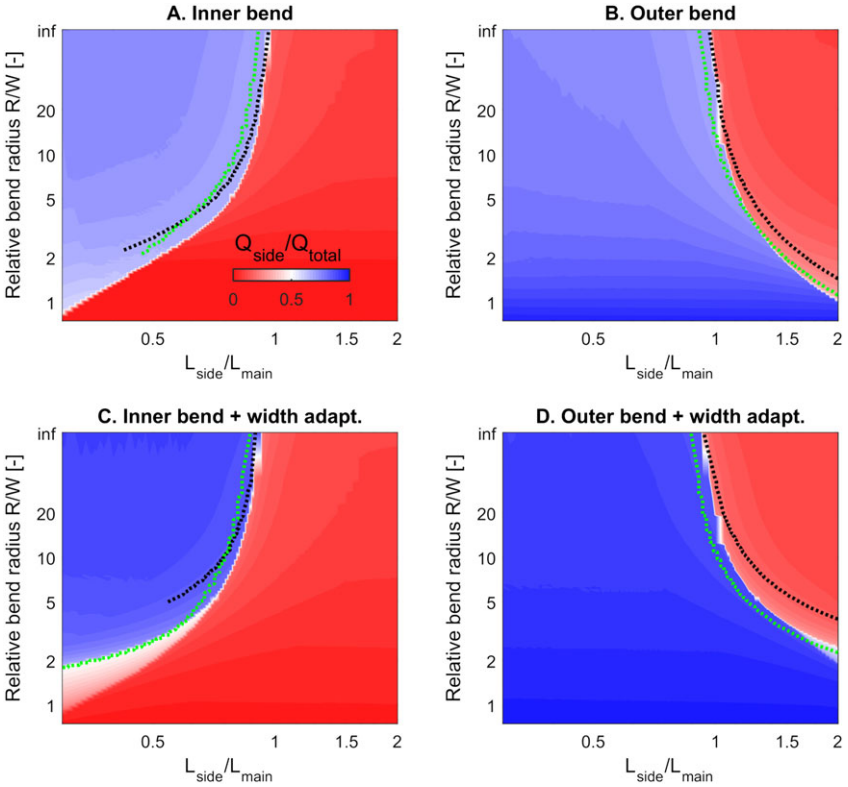

Figure 4. Equilibrium state of the two-channel system in the Wabash River (Figure 9) depending on the length difference between the channels, bend flow and width adaptation. The relative bend radius (*y*-axis) is defined as the ratio between the radius and the width of the upstream channel. An infinite relative radius corresponds to a straight channel, and a smaller relative radius corresponds to a larger bend flow intensity. The *x*-axis shows the ratio between the side channel length and the main channel length. The blue colour means that the side channel becomes dominant and the red colour means the main channel remains dominant. The white line that separates the blue and red surfaces is a result of interpolation and represents the abrupt transition. The black and green dotted lines represent the abrupt transition for the river Ain and the Sacramento River respectively. [Colour figure can be viewed at wileyonlinelibrary.com]

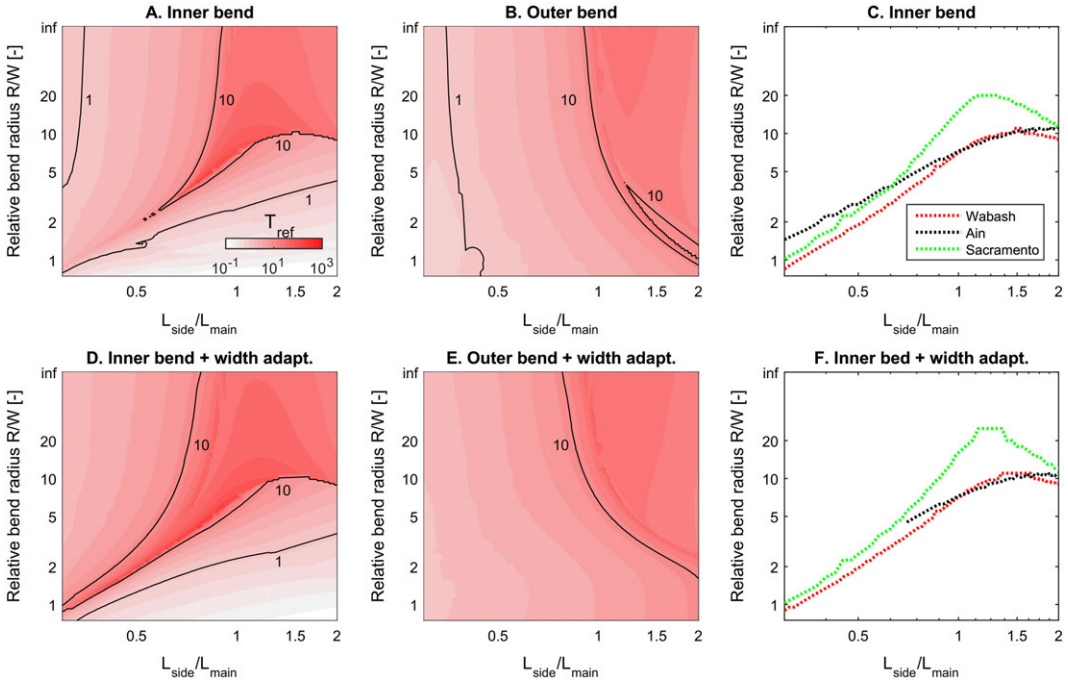

Figure 5. Timescale of the side channel development as defined in Figure 2 corresponding to Figure 4. Graphs C and F show the maximum timescale for three rivers derived from graphs A and D. [Colour figure can be viewed at wileyonlinelibrary.com]

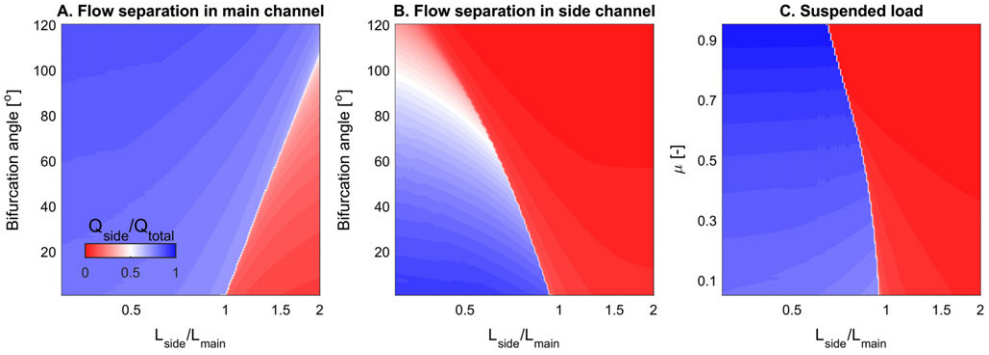

Figure 6. Equilibrium state of the two-channel system depending on the length difference between the channels, bifurcation angle and suspended sediment transport. The blue colour means that the side channel becomes dominant and the red colour means the main channel remains dominant. [Colour figure can be viewed at wileyonlinelibrary.com]

therefore do not show an infinite timescale. The line with the maximum timescale is shown in Figure 5C, F. This is not a stable situation; rather, a minor perturbation would initiate change. Below this line, the gradient in the timescale is much larger than above. This line occurs for similar conditions for each of the three rivers (Figure 5C, F). The timescale increases if width adaptation is accounted for and is in that case sensitive to the width adaptation timescale (Kleinhans *et al.*, 2011).

In the model the size of the flow separation zone is related to the bifurcation angle. Depending on the angle between the downstream channels and the upstream channel, a flow separation zone may occur in the main channel (Figure 6A) and in the side channel (Figure 6B). A large angle means a large flow separation zone that reduces the channel width at the entrance and therefore reduces the discharge in that channel, which results in aggradation. The computations with a flow separation zone in the side channel (Figure 6B) show a transition zone between a dominant main channel and a dominant side channel. The large transverse bed slope, which is induced by scour at the entrance of the channel, results in a transverse sediment flux at the bifurcation that is large enough to balance the increased transport capacity of the side channel. The flow separation zone increases the likelihood that the channel in which flow separation occurs closes.

The partitioning of the suspended bed-material load is different from the partitioning of bed load and this affects the equilibrium state (Figure 6C). We vary the parameter μ, which is the fraction of the sediment that is affected by the transverse bed slope (y-axis). For $\mu = 0$ we deal with bed load only and for $\mu = 1$ the sediment partitioning is independent of the transverse bed slope. In the latter case, the sediment partitioning is similar to the water discharge partitioning and one of the branches fully closes. The transport capacity in the side channel increases with $i_b^{5/2}$, where i_b is the slope of the side channel, whereas the water discharge increases with $i_b^{1/2}$. This means that if the side channel is steep enough the transport capacity increases faster than the water discharge, leading to erosion of the side channel. In the case of $\mu = 1$ this is the mechanism that can lead to a dominant side channel. For $\mu < 1$ it is easier for the side channel to become dominant, because due to the transverse bed slope more sediment is diverted to the main channel.

Field cases

We apply the presented stability diagrams to four side channel systems. We study the side channel systems using aerial images and compare them with the 1D numerical results.

Mollon, river Ain (France)

The river Ain is located in the southeast of France and is a tributary of the river Rhône. The average annual discharge is 120 $m^3\ s^{-1}$ and the 2-year peak flow is 760 $m^3\ s^{-1}$ (Dieras *et al.*, 2013). The surface grain size varies between 15 and 46 mm (Rollet, 2007). Figure 7 shows a series of aerial images of a two-channel system in the river Ain near Mollon, France. In 1968 the two channels have similar lengths. The west channel aggrades over time and a bar forms at the entrance. From 1991 a meander forms in the east channel, as is visible in 1996. This meander induces a length difference between the channels. In 1996 the west channel reopens due to a chute incision (Dieras *et al.*, 2013). The water-level gradient over the west channel is larger than over the east channel due to their length difference. The west channel therefore attracts more discharge relative to its size, which leads to degradation in the west channel. The discharge in the east channel therefore decreases, which leads to aggradation. From 2003 the conveyance capacity is larger in the west channel than in the east channel, and in 2005 the east channel does not convey water during base flow (Dieras *et al.*, 2013). Vegetation growth has likely accelerated aggradation due to increased trapping of sediment (Figure 7, 2010). The images show a widening of the west channel, which seems to be due to the unstable and poorly cohesive banks (Piégay *et al.*, 2002).

Based on the stability diagrams (Figure 4), we hypothesise that the length difference between the two channels caused the switch from a dominant main channel to a dominant side channel (Table I). Based on Figure 4, we find that the length difference between the west and east channel is sufficient for the west channel to become dominant. The predicted timescale is of the order of 25 or 90 years, depending on whether width adaptation is included (Figure 5). The banks in the river Ain are unstable (Piégay *et al.*, 2002), which suggests that the width adaptation timescale might be overestimated, leading to an overestimation of the timescale of side channel development. This could be solved by calibrating the timescale of the width adaptation on the basis of data, and would put the modelled timescale between the two present values. We expect that mechanisms that are not accounted for in the model lead to the filling up of the channel: for example, aggradation of finer sediments and the trapping of vegetation.

Martinaz, river Ain (France)

A second two-channel system in the river Ain is found near the village of Martinaz. Between 1954 and 1968 a meander forms (Figure 8), which cuts into an already existing channel (Figure 8, 1954), forming the side channel system shown in 1968. The bifurcation is located at the downstream end of the bend. Bend flow, i.e. spiral flow that is directed toward the

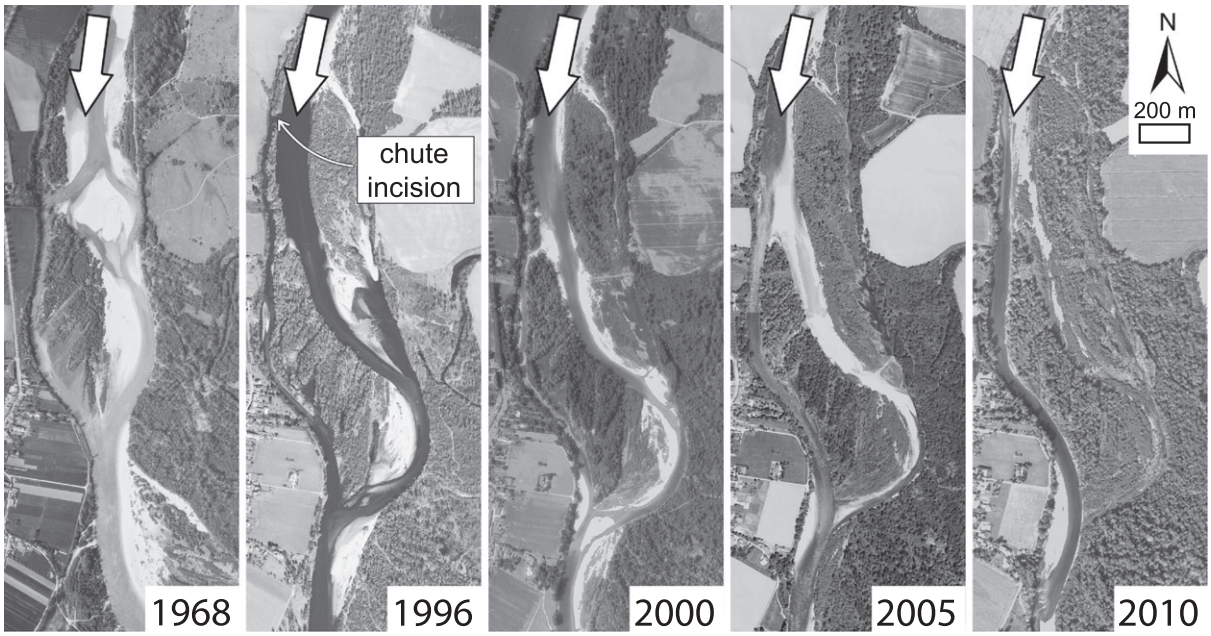

Figure 7. A series of aerial images of a two-channel system in the river Ain near Mollon, France. In 1995 the west channel is reopened, and around 2005 the east channel closes. (IGN France and Google Earth.).

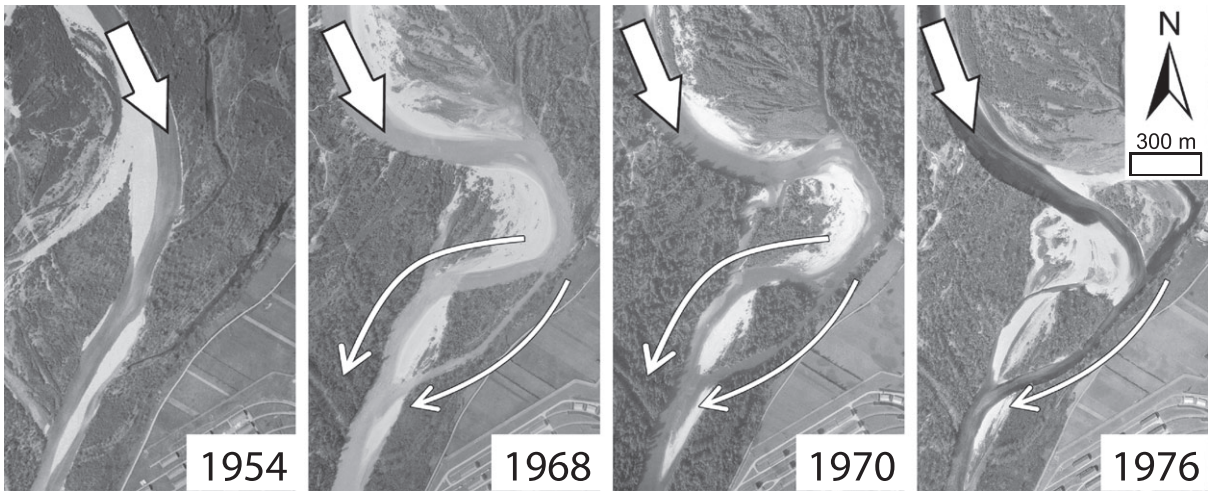

Figure 8. A series of aerial images of a two-channel system in the river Ain near Martinaz, France. A meander cuts into a former channel which is connected to the main channel in the outer bed (see image of 1968). The west channel starts to aggrade and the east channel becomes the main channel. (IGN France.).

inner bend near the bed, likely increases the sediment load into the west channel. In 1968 and 1970 a cutoff channel is visible in the meander. This cutoff does not become dominant, but may have affected the stability and the timescale of the side channel development. In 1976 another cutoff forms and the west channel aggrades such that it is disconnected from the main channel during base flow.

The development of the side channel system is likely affected by the bend flow at the bifurcation and the cutoff of the bend in 1968 and 1970. The numerical model results (Figure 4) show that the small length difference is sufficient for the east channel to become dominant and that bend flow increases the water discharge conveyed by the east channel. Including these two mechanisms and width adaptation in the numerical model yields a timescale of the order of 10 years to reach its equilibrium, which is comparable to the 8–10 years after which the west channel seems to have been disconnected (Figure 8).

Mackey Bend, Wabash River (USA)

The Wabash River is located on the border of Illinois and Indiana (USA). The average annual discharge is 825 m^3 s^{-1} and the 2-year flood is 3795 m^3 s^{-1} (Zinger *et al.*, 2013). Mackey Bend is located just upstream of the confluence between the Wabash River and the Ohio River (Figure 9, 2007A). In June 2008, a large discharge in the Wabash River in combination with a low discharge in the Ohio River leads to the formation of a cutoff channel (Zinger *et al.*, 2013). The bifurcation angle of 82° (Zinger *et al.*, 2013) leads to flow separation at the left bank of the cutoff channel. A bar forms in the flow separation zone (Figure 9, 2009). The first cutoff channel is shorter than the meander and therefore the cutoff attracts a relatively large discharge. The large flow velocity, in combination with the large flow separation zone, appears to result in bank erosion, allowing the channel to migrate and to reduce the bifurcation angle to about 60° in 2009.

Figure 9. A series of aerial images of a meander cutoff in the Mackey Bend of the Wabash River, USA. The first image (2007A) shows the full river bend and the confluence with the Ohio River in the bottom right corner. The other images are zoomed in on the location of the cutoffs. The first cutoff occurs in 2008 and the second in 2009. The second cutoff becomes the main channel. The former meander channel and the first cutoff slowly fill with sediment. (NAIP.). [Colour figure can be viewed at wileyonlinelibrary.com]

After several floods, a second cutoff channel forms in June 2009 (Zinger *et al.*, 2011). This new channel has an even larger water surface slope and therefore attracts a large fraction of the upstream water discharge. Measurements show that initially the bar in the flow separation zone remains small and bank migration is limited (Zinger *et al.*, 2013). During a moderate flood at the beginning of July 2010 the width increases rapidly and a bar forms in the flow separation zone, as shown in 2011. The two sharp corners in the banks, visible in 2010, possibly hinder the migration of the channel and the growth of the bar at the entrance. It is not clear why these seemingly hard corners in the banks occur. From 2011 the second cutoff channel conveys the larger part of the discharge and measurements show that during a flood event with a return period of 2 years in 2015 about 80% of the total discharge is conveyed by the second cutoff channel (Zinger, 2016).

The length difference and the bifurcation angle likely affected the development of the channels. The numerical model shows that very large bifurcation angles can outweigh the favourably short length of the side channels such that the main channel remains dominant (Figure 6B), but this only occurs if bank erosion is limited. The side channel system of the Wabash River shows extensive bank migration, which reduces the bifurcation angle. If we ignore the effect of the bifurcation angle, the timescale of the development of the first cutoff is about 2 years (Figure 5), which appears to be an underestimation on the basis of the aerial images. Possibly bar formation and bar-induced channel migration increased the timescale of the side channel development.

Colusa, Sacramento River (USA)

The Sacramento River is located in California (USA). Its average annual discharge is 350 $m^3\ s^{-1}$ and its 2-year flood is equal to 2100 $m^3\ s^{-1}$ (Constantine *et al.*, 2010). The average suspended load ($1.5 \times 10^6\ m^3\ yr^{-1}$) is much higher than the average bed load ($7.5 \times 10^4\ m^3\ yr^{-1}$), and is to a large extent transported as wash load (Singer and Dunne, 2004; Constantine *et al.*, 2010). A side channel system exists just upstream of the city of Colusa (Figure 10). Between 1964 and 1976 the west channel is connected to the main channel and it is much shorter than the east channel. We therefore expect the west channel to grow, but it only starts to do so after 1998. This may be due to a limited sediment transport in the river, barely erodible banks or the formation of a bar upstream of the bifurcation, which from 1993 may induce bend flow at the bifurcation. From 2009 the width of both channels is the same. We therefore expect that the conveyance capacity in the west channel is larger than in the east channel. In 2015 the sedimentation in the downstream part of the east channel almost closes the channel and we expect that the east channel closes in the next few years. This suggests a large difference in timescale between the opening of the west channel (in the order of 30 years) and the closing of the east channel (of the order of 10 years). Suspended bed-material load or even wash load may induce such a difference, as it requires space and time to settle. Suspended bed-material load has a limited effect on the opening of the west channel, but may determine the closing of the east channel. The role of suspended load seems to be confirmed by the 2015 image, which shows that aggradation starts near the downstream end of the east channel. This corresponds to the spatial lag expected for suspended load.

The large difference between bed load and suspended supply in the river likely affects the side channel development. Based on only bed load, the model predicts that the west channel becomes dominant and that the timescale of side channel development is of the order of 70 years (Figures 4 and 5). This corresponds to a switch of a dominant side channel to a dominant main channel after 35 years (Supplementary material, provided as supporting information). This agrees with the order of 30 years that was observed from the aerial images. However, the observed aggradation in the east channel is much faster than the model predicts. For equal channel slopes, suspended sediment that is less affected by the transverse bed slope than bed load tends to force the shallowest channel to close (Figure 6C). When a sufficient amount of water discharge is diverted into the west channel, suspended bed-material load may be able to settle in the east channel, which accelerates the side channel development, and this may explain the observed deposition in the downstream part of the east channel. The bend flow due to the bar that forms after 1993 might be an additional mechanism that diverts more sediment towards the

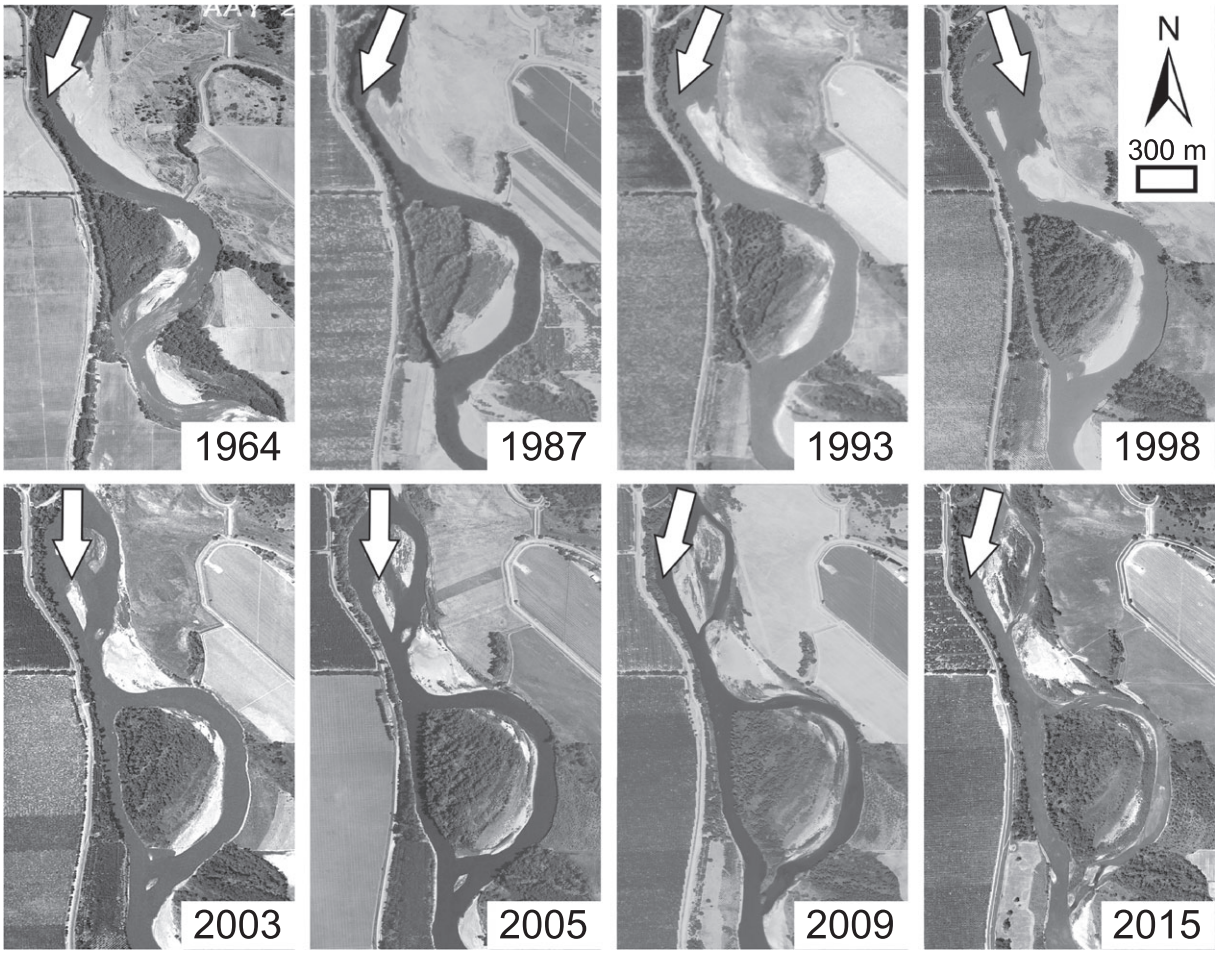

Figure 10. A series of aerial images of a meander cutoff upstream of Colusa in the Sacramento River, USA. The west channel increases in size and around 2009 the west channel seems to be the dominant channel. In 2015 large aggradation is visible in the east channel. (Geoportal California, NAPP USGS, NAIP and Google Earth.).

east channel. The images show that the relative bend radius varies between 1 and 2.5, which means that the timescale varies between 5 and 40 years.

Discussion

Our modelling study underlines the importance of a number of mechanisms affecting side channel development. The final stages of channel closure and its conversion to floodplain were not modelled. In this section we give an overview of the closing mechanisms that were not considered, the limitations of our method, and finally the applicability of the results to the designing of side channel systems.

Closing mechanisms

The four field cases show diverse behaviour. The aerial images are taken during base flow conditions and show that in a few cases one of the channels is disconnected from the main channel under base flow conditions, but the model does not reproduce this. We expect that silting up of the channels mainly occurs with fine sediment as in meander cutoff channels (Citterio and Piégay, 2009; Constantine *et al.*, 2010; Toonen *et al.*, 2012; Dieras *et al.*, 2013). Indeed, grain size measurements in the channels of the Wabash River clearly show that the bed of the closing channels consists of much finer sediment than the bed of the dominant channel (measurements from Zinger, 2016, and USACE). If the closing channel conveys limited discharge, for example in the case of a plugbar at the bifurcation, the connectivity at the confluence becomes important. When the discharge in the main channel varies, flow reversal can occur in the side channel and then new sediment is delivered to the closing channel through the confluence. This can increase the aggradation rate of such channels (Citterio and Piégay, 2009; Le Coz *et al.*, 2010).

A second mechanism that may induce or enhance aggradation in the closing channel is vegetation. Vegetation encroachment and settling is a mechanism that can induce aggradation in the channel. Vegetation increases the hydraulic roughness, creates a zone characterized by a smaller flow velocity and traps sediment (Makaske *et al.*, 2002; Rodrigues *et al.*, 2006; Baptist *et al.*, 2007; Van Oorschot *et al.*, 2015). The growth of vegetation depends, for example, on the flow depth, bed-level change and the flow velocity (Van Oorschot *et al.*, 2015). The flow depth and flow velocity in the closing channel may be small enough for vegetation to settle. We expect that in the side channel near Mollon (Figure 7) vegetation affects morphodynamic change. In closing channels conditions generally favour vegetation growth and therefore trapping of sediment.

Limitations of the numerical model and the use of aerial images

There are many uncertainties in the use of the 1D numerical model. Some of the relevant mechanisms are not included or

strongly simplified. 2D and 3D flow patterns that are important at the bifurcation are parametrized. Significant uncertainty follows from the nodal point relation that is a function of the transverse bed slope relation. Large differences can be found between transverse bed slope relations (Bolla Pittaluga *et al.*, 2015; Baar *et al.*, 2017) and this affects the stability of the bifurcation. A weaker transverse bed slope effect means that the side channel system is less stable and it is more difficult for the side channel to become dominant, because less sediment is diverted into the main channel (similarly to Figure 6C). The second source of transverse sediment flux is bend flow. The parametrization of bend flow assumes that spiral flow is fully developed and that flow separation does not occur. This implies that the effect of bend flow may be overestimated especially for small radii (Blanckaert and De Vriend, 2004). Other sources of uncertainties in our model are the bifurcation angle and the width adaptation parametrizations. Regardless of this, the model seem to be able to reproduce the development of side channel systems, and previous studies show that the model is able to reproduce the bifurcation development reasonably well (Kleinhans *et al.*, 2008, 2011; Van Dijk *et al.*, 2014; Gupta *et al.*, 2014; Bolla Pittaluga *et al.*, 2015).

The use of aerial images in studying the development of side channels has some limitations. In the case of the Wabash River, measurements were available on the flow velocity and the water discharge partitioning, but for the other cases assumptions were made based on the river geometry and the observed morphodynamic change. In addition, the aerial images do not provide information on the discharge partitioning and the bed-level variation. We therefore assume an initial water discharge partitioning and derive the initial bed level from this estimate. The aerial images are taken with irregular frequency, which means that processes that occur on short timescales are not visible. In addition, there is no reason to assume that the last recorded image represents the equilibrium state of the side channel system. The 1D numerical model always approaches and reaches an equilibrium, but, for example, temporally variable boundary conditions and meander formation, which are not included in the numerical model, affect the stability and the development of the side channel system and likely lead to a dynamic equilibrium state.

Application possibilities

Our stability diagrams provide a first insight on best practices for the design of a constructed side channel. As an example we consider a case where the required design is such that the main channel remains dominant and that slow side channel development is beneficial. This implies that it is preferable to design the side channel to be longer than the main channel, and preferably downstream of an outer bend or at the inside of a mild bend (Figure 4). This leads to the largest timescales of side channel development and the main channel remains dominant. This recommendation is unaffected by flow separation in the side channel or a large influence of suspended bed-material load. Flow separation in the main channel should be avoided, as it tends to form a dominant side channel (Figure 6A).

Generally, structures are placed in constructed side channels to control the discharge partitioning. The effect of structures is not included in the current 1D analysis and a better understanding of their influence on morphodynamic change is needed for a more accurate estimation of the timescale of side channel development.

Whether a maintenance-free side channel exists has yet to be determined. The numerical model suggests that a stable bifurcation exists in which the side channel remains open, but we did not account for floodplain-forming processes that may lead to full closure. Conceivably, side channels that gradually transform to floodplain could be ecologically valuable enough to outweigh the costs for maintenance.

Conclusions

Several mechanisms determine the equilibrium state of a side channel, development and characteristic timescale. Typically, the length of the side channel is an important parameter: a shorter side channel is more likely to become dominant and decreases the timescale of the side channel development. However, other mechanisms may outbalance or reduce the effect of a length difference. Bend flow increases the sediment load to one of the branches, the transverse bed slope can stabilize the side channel system, the flow separation zone decreases the water discharge to one of the branches, and suspended load reduces the effect of the transverse bed slope. Bank erosion hardly affects the equilibrium state, but causes larger timescales of side channel development depending on bank erodibility.

The 1D numerical results reproduce the morphological development and timescale of four side channels observed in multitemporal imagery. Furthermore, these cases demonstrate that the mechanisms are quite similar between sand-bed and gravel-bed rivers. Generalized results can therefore be used to assess the development and corresponding timescale for various side channel designs.

Acknowledgements— This research is supported by the Netherlands Organization for Scientific Research (NWO), which is partly funded by the Ministry of Economic Affairs, under grant number P12-P14 (RiverCare Perspective Programme) project number 13516. This research has benefited from cooperation within the network of the Netherlands Centre for River Studies. An anonymous reviewer and Bart Makaske are acknowledged for valuable comments that helped to improve the paper.

Appendix A: Equations of the 1D Numerical Model

Bolla Pittaluga *et al.* (2003) propose a mass balance over two computational cells upstream of the bifurcation:

$$Q_{s2} = Q_{s1}\frac{W_2}{W_2 + W_3} + q_{sy}\alpha_W W_1 \tag{A1}$$

where q_{sy} is the transverse sediment transport rate and $\alpha_W W_1$ is the distance upstream of the bifurcation over which the transverse sediment flux occurs. The factor α_W is assumed to vary between 2 and 3 based on physical and numerical experiments (Bolla Pittaluga *et al.*, 2003; Kleinhans *et al.*, 2008). The transverse sediment flux is computed by calculating a deflection angle of sediment in a longitudinal direction:

$$q_{sy} = \tan\beta_s \frac{Q_{s1}}{W_1} \tag{A2}$$

where β_s is the deflection angle of the sediment transport flux. This angle is given by (Koch and Flokstra, 1981)

$$\tan\beta_s = \frac{\sin\beta_\tau - \frac{1}{f(\theta)}\frac{\partial\eta}{\partial y}}{\cos\beta_\tau - \frac{1}{f(\theta)}\frac{\partial\eta}{\partial x}} \tag{A3}$$

where β_τ is the angle between the direction of the bed shear stress and the streamwise direction, $\partial\eta/\partial y$ is the transverse bed slope, $\partial\eta/\partial x$ is the longitudinal bed slope and $f(\theta)$ is a ratio between the fluid drag and the gravity forces on a particle (Talmon *et al.*, 1995):

$$f(\theta) = 9(D/h_1)^{0.3}\sqrt{\theta} \tag{A4}$$

where D is the sediment diameter, θ is the Shields stress, and h_1 is the water depth in the upstream channel. The angle of the shear stress (β_τ) is given by the transverse velocity and the effect of the spiral flow due to a river bend (Struiksma *et al.*, 1985):

$$\beta_\tau = \arctan\left(\frac{v}{u}\right) - \arctan\left(A\frac{W_{\min}}{W_{\max}}\frac{h_1}{R}\right) \tag{A5}$$

where v and u are the depth-averaged transverse and longitudinal flow velocity respectively, A is the spiral flow intensity and R is the radius of curvature of the streamlines (Kleinhans *et al.*, 2008). This radius is assumed to be similar to the radius of the centreline of the channel. In the case of a large difference in channel width between the downstream channels, a smaller portion of sediment transport rate that is affected by the spiral flow is transported over the interface between the two computational cells. Therefore, a damping factor ($W_{\min}/W_{\max}$) is added (Kleinhans *et al.*, 2011), which is the ratio between the width of the downstream channels. The spiral flow intensity is given by (Struiksma *et al.*, 1985)

$$A = \frac{2\epsilon}{\kappa^2}\left(1 - \frac{\sqrt{g}}{\kappa C}\right) \tag{A6}$$

where κ is the Von Kármán constant, C is the Chézy coefficient and ϵ is a calibration coefficient ($\epsilon \approx 1$). It is assumed that the spiral flow is fully developed, the bend is smooth and the radius so large that flow separation does not occur. The depth-averaged transverse velocity (v) is derived from the transverse discharge (Q_y). This transverse discharge arises from the fact that the discharge partitioning over the bifurcates generally differs from the width ratio of the bifurcates (Bolla Pittaluga *et al.*, 2003).

$$Q_y = \frac{1}{2}\left(Q_2 - Q_3 - Q_1\frac{W_2 - W_3}{W_2 + W_3}\right) \tag{A7}$$

The width adaptation is incorporated by assuming an empirical equilibrium width as a function of the water discharge (Kleinhans *et al.*, 2011):

$$W_{\text{eq}} = \gamma Q^{\beta_W} \tag{A8}$$

where W_{eq} is the equilibrium bankfull width, γ is estimated based on the upstream channel and $\beta_W \approx 0.5$ (Van den Berg, 1995). The change in the width is given by (Miori *et al.*, 2006; Kleinhans *et al.*, 2011)

$$\frac{\partial W}{\partial t} = \frac{W_{\text{eq}} - W}{T_W} \tag{A9}$$

where W is the actual channel width and T_W represents the timescale over which the width adjustment occurs. The timescale is given by (Kleinhans *et al.*, 2011)

$$T_W = \alpha_{T_W}\frac{Wh}{q_{s,\text{bank}}} \tag{A10}$$

where $q_{s,\text{bank}}$ is a fraction of the total streamwise sediment transport per unit width (q_s) that contributes to bank retreat or aggradation, α_{T_W} is a calibration parameter and Wh represents the volume of sediment per unit length of the channel. The sediment transport rate near the bank ($q_{s,\text{bank}}$) is assumed to be $q_{s,\text{bank}} = q_s h/W$ (Kleinhans *et al.*, 2011). This is an initial estimate of the timescale, in which local characteristics of the banks are not taken into account. The eroded or deposited sediment from the banks is conserved by adding an additional source/sink term to the Exner conservation law:

$$(1-p)\frac{\partial\eta}{\partial t} - \frac{\partial q_s}{\partial x} = \frac{\partial W}{\partial t}\frac{W}{h} \tag{A11}$$

where p is the porosity of the bed sediment and η is the bed level.

References

Baar AW, Weisscher SAH, Uijttewaal WSJ, Kleinhans MG. 2017. Sediment transport processes on transverse bed slopes. In *NCR Days 2017 Book of Abstracts*, Hoitink AJF, De Ruijsscher TV, Geertsema TJ, Makaske B, Wallinga J, Candel JHJ, Poelman J (eds), NCR: Wageningen, the Netherlands; 50–51.

Baptist MJ, Babovic V, Rodríguez Uthurburu J, Keijzer M, Uittenbogaard RE, Mynett A, Verwey A. 2007. On inducing equations for vegetation resistance. *Journal of Hydraulic Research* **45**: 435–450.

Bertoldi W, Tubino M. 2007. River bifurcations: experimental observations on equilibrium configurations. *Water Resources Research* **43**. https://doi.org/10.1029/2007WR005907.

Blanckaert K, De Vriend HJ. 2004. Secondary flow in sharp open-channel bends. *Journal of Fluid Mechanics* **498**: 353–380.

Bolla Pittaluga M, Repetto R, Tubino M. 2003. Channel bifurcation in braided rivers: equilibrium configurations and stability. *Water Resources Research* **39**. https://doi.org/10.1029/2001WR001112.

Bolla Pittaluga M, Coco G, Kleinhans MG. 2015. A unified framework for stability of channel bifurcations in gravel and sand fluvial systems. *Geophysical Research Letters* **42**: 7521–7536.

Bravard JP. 1986. La basse vallée de l'Ain: dynamique fluviale appliquée à l'écologie. In *Documents de cartographie écologique, recherches interdisciplinaires sur les écosystèmes de la basse-plaine de l'Ain (France): potentialités évolutives et gestion*, Roux AL (ed), Vol. 29, Laboratoire de biologie végétale: Grenoble; 17–43.

Bridge JS. 2003. *Rivers and Floodplains: Forms, Processes, and Sedimentary*. Blackwell Science: Oxford.

Bulle H. 1926. *Untersuchungen über die Geschiebeableitung bei der Spaltung von Wasserlüfen*. VDI: Berlin.

Church M. 2006. Bed material transport and the morphology of alluvial river channels. *Annual Review of Earth and Planetary Sciences* **34**: 325–354.

Citterio A, Piégay H. 2009. Overbank sedimentation rates in former channel lakes: characterization and control factors. *Sedimentology* **56**: 461–482.

Constantine JA, Dunne T, Piégay H, Kondolf GM. 2010. Controls on the alluviation of oxbow lakes by bed-material load along the Sacramento River, California. *Sedimentology* **57**: 389–407.

De Heer A, Mosselman E. 2004. Flow structure and bedload distribution at alluvial diversions. In *River Flow 2014*, Greco M, Carravetta A, Della Morte R (eds): Naples, Italy; 801–806.

Dieras PL, Constantine JA, Hales TC, Piégay H, Riquier J. 2013. The role of oxbow lakes in the off-channel storage of bed material along the Ain River, France. *Geomorphology* **188**: 110–119.

Dietrich WE, Smith JD. 1984. Bed load transport in a river meander. *Water Resources Research* **20**: 1355–1380.

Dutta S, Wang D, Tassi P, Garcia MH. 2017. Three-dimensional numerical modeling of the Bulle effect: the nonlinear distribution of near-bed sediment at fluvial diversions. *Earth Surface Processes and Landforms* **42**: 2322–2337. https://doi.org/10.1002/esp.4186.

Edmonds DA, Slingerland RL. 2008. Stability of delta distributary networks and their bifurcations. *Water Resources Research* **44**. https://doi.org/10.1029/2008wr006992.

Engelund F, Hansen E. A monograph on sediment transport in alluvial streams, Tekniskforlag Copenhagen, 1967.

Formann E, Habersack HM, Schober S. 2007. Morphodynamic river processes and techniques for assessment of channel evolution in Alpine gravel bed rivers. *Geomorphology* **901**: 340–355.

Frings RM, Kleinhans MG. 2008. Complex variations in sediment transport at three large river bifurcations during discharge waves in the river Rhine. *Sedimentology* **55**: 1145–1171.

Gaweesh A, Meselhe E. 2016. Evaluation of sediment diversion design attributes and their impact on the capture efficiency. *Journal of Hydraulic Engineering* **142**. https://doi.org/10.1061/(ASCE)HY.1943-7900.0001114.

Gupta N, Kleinhans MG, Addink EA, Atkinson PM, Carling PA. 2014. One-dimensional modeling of a recent Ganga avulsion: assessing the potential effect of tectonic subsidence on a large river. *Geomorphology* **213**: 24–37.

Hardy RJ, Lane SN, Yu D. 2011. Flow structures at an idealized bifurcation: a numerical experiment. *Earth Surface Processes and Landforms* **36**: 2083–2096.

Helfield JM, Engstrom J, Michel JT, Nilsson C, Jansson R. 2012. Effects of river restoration on riparian biodiversity in secondary channels of the Pite River, Sweden. *Environmental Management* **49**: 130–141.

Henry CP, Amoros C, Giuliani Y. 1995. Restoration ecology of riverine wetlands: II. An example in a former channel of the Rhône River. *Environmental Management* **19**: 903–913. https://doi.org/10.1007/bf02471941.

Kästner K, Hoitink AJF, Vermeulen B, Geertsema TJ, Ningsih NS. 2017. Distributary channels in the fluvial to tidal transition zone. *Journal of Geophysical Research – Earth Surface* **122**: 696–710.

Kleinhans MG, Jagers HRA, Mosselman E, Sloff CJ. 2008. Bifurcation dynamics and avulsion duration in meandering rivers by one-dimensional and three-dimensional models. *Water Resources Research* **44**. https://doi.org/10.1029/2007WR005912.

Kleinhans MG, Cohen KM, Hoekstra J, IJmker JM. 2011. Evolution of a bifurcation in a meandering river with adjustable channel widths, Rhine delta apex, The Netherlands. *Earth Surface Processes and Landforms* **36**: 2011–2027.

Kleinhans MG, Ferguson RI, Lane SN, Hardy RJ. 2013. Splitting rivers at their seams: bifurcations and avulsion. *Earth Surface Processes and Landforms* **38**: 47–61.

Koch FG, Flokstra C. 1981. Bed level computations for curved alluvial channels. In *Proceedings of the XIXth congress of the International Association for Hydraulic Research, 2-7 Feb. 1981*, Vol. 2: New Delhi, India; 357–364.

Konsoer KM. 2014. *Influence of riparian vegetation on near-bank flow structure and rates of erosion on a large meandering river*. PhD thesis, University of Illinois, Urbana-Champaign, USA.

Le Coz J, Michalková M, Hauet A, Comaj M, Dramais G, Holubová K, Piégay H, Paquier A. 2010. Morphodynamics of the exit of a cutoff meander: experimental findings from field and laboratory studies. *Earth Surface Processes and Landforms* **35**: 249–261.

Makaske B, Smith DG, Berendsen HJA. 2002. Avulsions, channel evolution and floodplain sedimentation rates of the anastomosing upper Columbia River, British Columbia, Canada. *Sedimentology* **49**: 1049–1071.

Mendoza A, Abad JD, Frias CE, Ortals C, Paredes J, Montoro H, Vizcarra J, Simon C, Soto-Cortes G. 2016. Planform dynamics of the Iquitos anabranching structure in the Peruvian Upper Amazon River. *Earth Surface Processes and Landforms* **41**: 961–970.

Miori S, Repetto R, Tubino M. 2006. A one-dimensional model of bifurcations in gravel bed channels with erodible banks. *Water Resources Research* **42**. https://doi.org/10.1029/2006wr004863.

Nabet F. 2014. *Etude du réajustement du lit actif en Loire moyenne, bilan géomorphologique et diagnostic du fonctionnement des chanaux secondaires en vue d'une gestion raisonnée*. PhD thesis, Université Panthéon–Sorbonne, Paris, France.

Olivier JM, Dole-Olivier MJ, Amoros C, Carrel G, Malard F, Lamouroux N, Bravard JP. 2009. The Rhône river basin. In *Rivers of Europe*, Tockner K, Uehlinger U, Robinson CT (eds), Academic Press: Cambridge, MA; 247–295.

Parker G. 2004. 1d sediment transport morphodynamics with applications to rivers and turbidity currents. E-book. Available: http://hydrolab.illinois.edu/people/parkerg/morphodynamics_e-book.htm [15 October 2017].

Piégay H, Bornette G, Grante P. 2002. Assessment of silting-up dynamics of eleven cut-off channel plugs on a free meandering river (Ain River, France). In *Applied Geomorphology: Theory and Practice*, Allison R (ed), Vol. 10, Wiley: Chichester; 227–247.

Riad K. 1961. *Analytical and experimental study of bed load distribution at alluvial diversions*. PhD thesis, Delft University of Technology, Delft, the Netherlands.

Rodrigues S, Bréhéret JG, Macaire JJ, Moatar F, Nistoran D, Jugé P. 2006. Flow and sediment dynamics in the vegetated secondary channels of an anabranching river: the Loire River (France). *Sedimentary Geology* **186**: 89–109.

Rollet AJ. 2007. *Etude et gestion de la dynamique sédimentaire d'un tronçon fluvial à l'aval d'un barrage: le cas de la basse vallée de l'Ain*. PhD thesis, L'Université Jean Moulin Lyon 3, Lyon, France.

Schiemer F, Baumgartner C, Tockner K. 1999. Restoration of floodplain rivers: the Danube restoration project. *Regulated Rivers: Research and Management* **15**: 231–244.

Simons JHEJ, Bakker C, Schropp MHI, Jans LH, Kok FR, Grift RE. 2001. Man-made secondary channels along the River Rhine (The Netherlands): results of post-project monitoring. *Regulated Rivers: Research and Management* **17**: 473–491. https://doi.org/10.1002/rrr.661.

Singer MB, Dunne T. 2004. Modeling decadal bed material sediment flux based on stochastic hydrology. *Water Resources Research* **40**. https://doi.org/10.1029/2003WR002723.

Slingerland R, Smith ND. 1998. Necessary conditions for a meandering-river avulsion. *Geology* **26**: 435–438.

Slingerland R, Smith ND. 2004. River avulsions and their deposits. *Annual Review of Earth and Planetary Sciences* **32**: 257–285.

Sloff CJ, Mosselman E. 2012. Bifurcation modelling in a meandering gravel-sand bed river. *Earth Surface Processes and Landforms* **37**: 1556–1566.

Sloff CJ, Bernabè M, Baur T. 2003. On the stability of the Pannerdensche Kop river bifurcation. In *3rd IAHR Symposium River, Coastal and Estuarine Morphodynamics*, Sánchez-Arcilla A, Bateman A (eds): Barcelona, Spain; 1001–1011.

Struiksma N, Olesen KW, Flokstra C, De Vriend HJ. 1985. Bed deformation in curved alluvial channels. *Journal of Hydraulic Research* **23**: 57–79.

Talmon AM, Struiksma N, Van Mierlo MCLM. 1995. Laboratory measurements of the direction of sediment transport on transverse alluvial-bed slopes. *Journal of Hydraulic Research* **33**: 495–517. https://doi.org/10.1080/00221689509498657.

Tockner K, Schiemer F, Ward JV. 1998. Conservation by restoration: the management concept for a river–floodplain system on the Danube River in Austria. *Aquatic Conservation: Marine and Freshwater Ecosystems* **8**: 71–86.

Toonen WHJ, Kleinhans MG, Cohen KM. 2012. Sedimentary architecture of abandoned channel fills. *Earth Surface Processes and Landforms* **37**: 459–472.

Van den Berg J H. 1995. Prediction of alluvial channel pattern of perennial rivers. *Geomorphology* **12**: 259–279.

Van der Mark CF, Mosselman E. 2013. Effects of helical flow in one-dimensional modelling of sediment distribution at river bifurcations. *Earth Surface Processes and Landforms* **38**: 502–511.

Van Dijk WM, van de Lageweg WI, Kleinhans MG. 2012. Experimental meandering river with chute cutoffs. *Journal of Geophysical Research* **117**. https://doi.org/10.1029/2011jf002314.

Van Dijk WM, Schuurman F, Van de Lageweg WI, Kleinhans MG. 2014. Bifurcation instability and chute cutoff development in meandering gravel-bed rivers. *Geomorphology* **213**: 277–291.

Van Oorschot M, Kleinhans MG, Geerling G, Middelkoop H. 2015. Distinct patterns of interaction between vegetation and morphodynamics. *Earth Surface Processes and Landforms* **41**: 791–808. https://doi.org/10.1002/esp.3864.

Van Rijn LC. 1993. *Principles of Sediment Transport in Rivers, Estuaries and Coastal Seas*. Aqua: Amsterdam.

Wang ZB, De Vries M, Fokkink RJ, Langerak A. 1995. Stability of river bifurcations in 1d morphodynamic models. *Journal of Hydraulic Research* **33**: 739–750.

Zinger JA. 2016. *From meander bend to oxbow lake: morphodynamics and sedimentology of chute cutoffs*. PhD thesis, University of Illinois, Urbana-Champaign, USA.

Zinger JA, Rhoads BL, Best JL. 2011. Extreme sediment pulses generated by bend cutoffs along a large meandering river. *Nature Geoscience* **4**: 675–678.

Zinger JA, Roads BL, Best JL, Johnson KK. 2013. Flow structure and channel morphodynamics of meander bend chute cutoffs: a case study of the Wabash River, USA. *Journal of Geophysical Research – Earth Surface* **118**: 2468–2487.

Supporting Information

Supporting information may be found in the online version of this article.

